Electronic Structure of the Water Dimer Cation

Piotr A. Pieniazek,[†] Joost VandeVondele,[‡] Pavel Jungwirth,*[,§] Anna I. Krylov,*[,†] and Stephen E. Bradforth[†,*]

Department of Chemistry, University of Southern California, Los Angeles, California 90089-0482, Physical Chemistry Institute, Zurich University, Winterthurerstrasse 190, CH-8057 Zurich, Switzerland, and Institute of Organic Chemistry and Biochemistry, Academy of Sciences of the Czech Republic, and Center for Biomolecules and Complex Molecular Systems, Flemingovo nám. 2, 16610 Prague 6, Czech Republic

Received: March 11, 2008; Revised Manuscript Received: April 29, 2008

The spectroscopic signatures of proton transfer in the water dimer cation were investigated. The six lowest electronic states were characterized along the reaction coordinate using the equation-of-motion coupled-cluster with single and double substitutions method for ionized systems. The nature of the dimer states was explained in terms of the monomer states using a qualitative molecular orbital framework. We found that proton transfer induces significant changes in the electronic spectrum, thus suggesting that time-resolved electronic femtosecond spectroscopy is an effective strategy to monitor the dynamics following ionization. The electronic spectra at vertical and proton-transferred configurations include both local excitations (features similar to those of the monomers) and charge-transfer bands. Ab initio calculations were used to test the performance of a self-interaction correction for density functional theory (DFT). The corrected DFT/BLYP method is capable of quantitatively reproducing the proper energetic ordering of the $(H_2O)_2^+$ isomers and thus is a reasonable approach for calculations of larger systems.

1. Introduction

Ionized states in condensed media, for example, those produced by radiation in biological tissue, or encountered in the storage and reprocessing of fissioned nuclear materials are not yet fully understood.[1–3] Even radiolysis of water, a predominant molecular target of the incident radiation in these situations, which has also served as the prototypical system for disentangling the phenomenology of high-energy processes in bulk liquids, has not been completely mapped out. For example, the nature of the initially excited states and sub-50-fs ionization/dissociation dynamics after deposition of energy have not been directly observed.[3]

The major ionization channel in water radiolysis includes the following steps:

$$n\mathrm{H_2O} \rightarrow (\mathrm{H_2O})_n^* \rightarrow \mathrm{H_2O^+(H_2O)}_{n-1} + \mathrm{e^-} \rightarrow \ldots \rightarrow \mathrm{H_3O^+_{aq}} + \mathrm{OH_{aq}} + \mathrm{e^-_{aq}} \quad (1)$$

The extent of delocalization of the initial excitation, that is, the number n of water molecules participating in $(H_2O)_n^*$, and the character of the charged species immediately after charge separation are poorly defined. Both quantities are likely to depend on the initial energy deposited.[4] In addition to reaction 1, energy deposited into water can also lead to homolytic bond breaking yielding H + OH, which resembles the gas phase photodissociation.[5] Besides the practical interest in the yields and spatial distribution of reactive radical products, this system also presents several fundamental questions on the mechanism and dynamics of separation and delocalization of both charge and spin in a partially disordered and rapidly fluctuating system.

Both the electronic structure and molecular dynamics of water are amenable to simulation. Although the structure, dynamics, and spectroscopy of the excess electron have been investigated extensively, modeling the other initial product of photoionization,[6,7] the ionized hole, has not been attempted in bulk, although cluster studies were reported.[8–11] The delocalization of the initial charge, the timescale, and dynamics of reaction 1, as well as the fate and separation of the products are all important issues that a simulation could help to explain. Our ongoing efforts to simulate the excess hole in bulk require the benchmarking of electronic structure methods for ab initio molecular dynamics (AIMD). One of the goals of the present study is to compare reliable calculations of the simplest fragment of the hole in water, the water dimer cation, against computationally less demanding methods suitable for AIMD.[12]

Moreover, in the laboratories of one of us, photolysis studies of pure water have been carried out with pulses as short as 25 fs. With this time resolution, femtosecond pump-probe spectroscopy should be able to track the proton-transfer step in reaction 1 and with a dispersed probe covering continuously the near UV and visible, the transients should be identifiable by their spectroscopic signatures. However, it is critical to establish the signature of the H_2O^+ intermediate and distinguish it from the subsequent species such as $(OH\cdots H_3O^+)$ and $OH_{(aq)}$.[13,14] Therefore, another major goal of this work is to describe the excited states of each of these species accurately, at least in small clusters. This will allow an assessment of what information electronic spectroscopy can provide in tracking the ionization chemistry of bulk water. Our theoretical approach parallels a recent study we performed on the electronic spectroscopy of the benzene dimer cation, a core species in the ionization of liquid benzene.[15]

* Corresponding authors. E-mail: pavel.jungwirth@uochb.cas.cz (P.J.), krylov@usc.edu (A.K.), and bradfort@usc.edu (S.B.).
† University of Southern California.
‡ Zurich University.
§ Institute of Organic Chemistry and Biochemistry, Academy of Sciences of the Czech Republic, and Center for Biomolecules and Complex Molecular Systems.

10.1021/jp802140c CCC: $40.75
Published on Web 06/18/2008

The results for a gas-phase water dimer establish a foundation for understanding the ionized water in the condensed phase. Moreover, the gas-phase species is also of interest and has attracted experimental and theoretical attention in the past, albeit not in the the context of its electronic spectroscopy. Ng et al.[16] determined the adiabatic ionization energy (IE) to be 11.2 eV by photoionization threshold measurements. De Visser[17] and coworkers investigated the reactivity of $(H_2O)_2^+$ towards a series of substrates, placing the adiabatic IE in the 10.8−10.9 eV bracket. Achiba and co-workers[18] measured the photoelectron spectra of $(H_2O)_2^+$, providing information about the two lowest electronic states of the cation. They observed two broad peaks centered at 12.1 and 13.2 eV and determined the onset of ionization to be at 11.1 eV. This work spurred a series of theoretical studies.[19–25] Although the first ionization was assigned as ionization from the out-of-plane orbital of the donor molecule, there was a controversy as to the site of second ionization. Early study pointed to ionization of the a_1 donor orbital, but subsequent correlated calculations reassigned it to the b_1 acceptor orbital.[23] Also, 2D potential energy surface (PES) cuts for the proton-transfer reaction along the O−O and O−H coordinates were calculated.[22] Density functional theory (DFT) calculations determined the lowest-energy isomer to be the hemibonded structure,[26,27] which later was shown to be an artifact of the self-interaction error (SIE).[28] Müller and coworkers studied ionization of small water clusters using Green's functions.[29] Their work focused on vertical structures and a hinted at the delocalized nature of the hole in the ground and excited states of water-cluster cations.

This work presents calculations for the water dimer cation at the geometry of the neutral water dimer and along the proton-transfer reaction coordinate to the $OH\cdots H_3O^+$ products. The character of the ground and the low-lying excited states are described within a Dimer Molecular Orbital-Linear Combination of Fragment Molecular Orbitals (DMO-LCFMO) framework. We also chart the electronic spectroscopy of the system as it evolves along the reaction coordinate. The predictions of this study will guide ongoing laboratory femtosecond studies and AIMD simulations of ionized bulk water.

2. Theoretical Methods and Computational Details

We begin by characterizing the monomer fragments and then proceed to the structures and excited states of water dimer cation. Theoretical descriptions of the ground and excited electronic states of doublet systems, like $(H_2O)_2^+$ or OH, are problematic because of symmetry breaking and spin-contamination of the doublet Hartree−Fock (HF) references.[30–32] Equation-of-motion coupled-cluster for ionization energies (EOM-IP-CC)[33–36] overcomes these difficulties by describing the problematic open-shell doublet wave functions Ψ(cation) as ionized/excited states of a well-behaved neutral wave function Ψ(neutral):

$$\Psi(\text{cation}) = \hat{R}\Psi(\text{neutral}), \tag{2}$$

where the Koopmans-like operator R generates all possible ionized, and ionized and simultaneously excited configurations out of the closed-shell reference determinant, and Ψ(neutral) is a coupled-cluster wave function, typically including only single and double substitutions (CCSD). Truncating R at $1h2p$ and $2h3p$ levels gives rise to the EOM-IP-CCSD and EOM-IP-CC(2,3) models, respectively. The latter model includes more correlation and is, therefore, more accurate. However, it is not practical for extensive calculations because of the higher computational cost, and we employ it in this work for benchmark purposes.

The geometries of the closed-shell species [H_2O, OH^-, H_3O^+, $(H_2O)_2$] were optimized at the second-order Møller−Plesset perturbation theory level with the 6-311++G** basis set (MP2/6-311++G**), whereas those of the open-shell doublet species [OH, proton-transferred and hemibonded $(H_2O)_2^+$], at the EOM-IP-CCSD/6−311++G** level. For the proton-transferred structure, both the C_s and the C_1 symmetry structures were obtained.

Monomer calculations of IEs were carried out, and their accuracy was assessed using the available experimental data. Calculations were performed at the EOM-IP-CCSD and EOM-IP-CC(2,3) levels using the 6-311++G** and aug-cc-pVTZ basis sets. On the basis of these benchmark results, the 6-311++G** basis set was selected for production calculations. Excitation energies and transition properties for monomer fragments and the dimer were computed using EOM-IP-CCSD and EOM-CCSD for excitation energies (EOM-EE-CCSD).[37–39] EOM-EE-CCSD allows one to investigate the possible presence of states derived by excitation to virtual orbitals and, therefore, not described by EOM-IP. EOM-EE results are also useful for assessing the accuracy of the excited state's description based on the open-shell reference. Additionally, excitation energies were obtained using EOM-IP-CC(2,3).

The character of the dimer excited states was characterized using the natural bond orbital (NBO) analysis[40] by calculating the natural charge of the fragments. The NBO analysis was also applied to the reference CCSD/6-311++G** wave functions. When appropriate, unrestricted HF (UHF) references were used in geometry optimizations, and restricted open-shell (ROHF) references were employed in evaluation of excitation energies and transition properties.

To characterize the proton-transfer reaction from the vertical ionized dimer, we computed a PES scan using EOM-IP-CCSD/6-311++G**, under the C_s symmetry constraint. To evaluate the consequences of this approximation, we compared C_1 and C_s configurations of the proton-transferred structure. Briefly, excitation energies are insensitive to this constraint, but intensities are sensitive to it. The distance between the oxygen atoms was varied between 2.30 and 3.10 Å, while the distance between the hydrogen of the H-bond donor and the oxygen of the acceptor was varied from 0.90 to 2.20 Å, with 0.05-Å increments. At each point, a constrained geometry optimization was conducted. Subsequently, the points corresponding to the neutral (A) and proton-transferred geometries (C) were identified on the grid. A steepest descent path was followed between A and C. Excitation energies and transition properties were computed along the path using EOM-IP-CCSD/6-311++G**.

All ab initio calculations were performed using the *Q-CHEM* ab initio package.[41] The basis sets were obtained from the EMSL repository.[42] The geometries are available as Supporting Information.

With the goal of ab initio Born−Oppenheimer molecular dynamics simulations of photoionization in bulk water,[12] we benchmarked the performance of DFT methods implemented within the *CP2K/Quickstep* software package.[43] In *CP2K/Quickstep*, DFT is implemented using a mixed Gaussian and plane-waves approach. We employed the BLYP functional with the double-ζ (DZVP) and triple-ζ (TZV2P) basis sets, along with the Goedecker−Teter−Hutter pseudo-potentials for oxygen 1s electrons.[44] The energy cutoff for plane waves was set to 280 Ry. Calculations for the radical cation were performed using unrestricted (UKS) and restricted open-shell (ROKS) Kohn−Sham schemes. To eliminate the errors due to electron self-interaction,[45–47] which are significant for open-shell and charge-transfer systems, we applied a self-interaction correction (SIC) within the ROKS

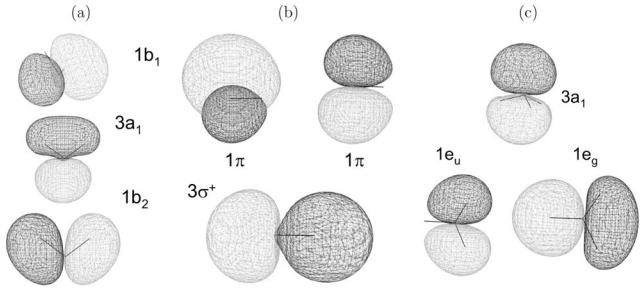

Figure 1. Three highest occupied MOs of (a) H_2O, (b) OH^-, and (c) H_3O^+. The geometric frame is rotated for each orbital to best show the orbital character.

method.[48–50] For SIC, we used the recommended values of 0.2 for Coulomb term scaling and zero for scaling of the exchange-correlation term.[49] For comparison and a stability check,we also employed a value of 0.2 for the latter scaling.

3. Results

3.1. Monomers. The DMO-LCFMO description (see the Appendix) of the dimer is based on the fragment orbitals and relevant excited states. In the water dimer cation, we are interested in the states derived by single ionization of the neutral. Thus, at the vertical geometry the DMOs can be expressed in terms of the occupied H_2O orbitals. The proton-transferred cation orbitals originate from the $OH^- \cdots H_3O^+$ dimer, and the OH^- and H_3O^+ occupied orbitals form a neutral basis. The three highest occupied molecular orbitals (MOs) of H_2O, OH^-, and H_3O^+ are shown in Figure 1, and the corresponding IEs are given in Table 1. Overall, the theory and the experiment, where available, agree well.

It is important to determine which of the monomer transitions are relevant to the dimer cation spectroscopy. The ground-state electronic structure at the proton-transferred geometry corresponds to the ionization of the hydroxyl part of the $OH^- \cdots H_3O^+$ dimer, as dictated by the IE considerations. The EOM-IP method restricts us to the electronic states derived by single ionizations of the neutrals. Thus, we only discuss transitions in the ionized system for which the singly occupied MO (SOMO) is the target orbital. This restricts the types of transitions to (i) the transitions within the OH moiety, (ii) the transitions from the H_3O^+ to the OH moiety, leading to the formation of $OH^- \cdots H_3O^{2+}$. The two groups can be related to the excited states of OH and H_3O^{2+} molecules, respectively. In contrast, excitations at the neutral vertical geometry always correspond to $H_2O^+ \cdots H_2O$, the charge being located on either the H-bond donor or the acceptor. Thus, one needs to consider only the states of H_2O^+. The excited states of the monomers are given in Table 2.

There are two possible excitations in H_2O^+ in the experimentally relevant energy range (1−6 eV). The $b_1 \leftarrow a_1$ transition is optically allowed and occurs at 2.3 eV, whereas the dipole-forbidden $b_1 \leftarrow b_2$ excitation is at 6.5 eV. The character of the electronic states does not change upon structural relaxation from the vertical neutral to the cation equilibrium geometry. The OH radical has only one excitation, $\pi \leftarrow \sigma$, at 4.2 eV. Addition of a proton to H_2O^+ produces H_3O^{2+}, which features a weak $a_1 \leftarrow e$ transition at 5.8 eV. Overall, addition/subtraction of a proton to/from H_2O^+ dramatically changes the nature of the MOs and the electronic transitions. Thus, each species has unique electronic states that cannot be described as perturbed H_2O^+ states.

The EOM-IP-CCSD method treats accurately the dimer cation states derived by single ionization of the neutral, whereas the cation states corresponding to excitation to a virtual orbital of the neutral are not well-described owing to their significant two-electron character. Neglecting these cation excitations is acceptable only if these states are outside the experimentally relevant spectral region. In the context of the water dimer cation at the geometry of the neutral species, we need to consider the excited states of H_2O^+ and H_2O. The lowest excited state of the water monomer in the gas phase is the $\tilde{A}^1 B_1$ state at 7.4−7.5 eV.[51] It is derived by excitation from the $1b_1$ to the $4a_1$/Rydberg 3s orbital. The first two excitations (2 and 6 eV) in H_2O^+ are excitations to the SOMO and are well-described by EOM-IP-CCSD. The next excited state, $2\ ^2B_1$, occurs at 13.7 eV as calculated by EOM-EE-CCSD/6-311++G**. At the proton-transferred configuration states of H_3O^+ and OH are relevant. The lowest excited state of H_3O^+, $2\ ^1A_1$, occurs at 11.8 eV (EOM-EE-CCSD/6-311++G**). The lowest OH excitation is $\sigma \leftarrow \pi$ at 4 eV and is described by EOM-IP-CCSD. The next one, to the $B\ ^2\Sigma^+$ state, is at 8.7 eV. Thus, monomer states not described by EOM-IP-CCSD are well outside the region probed in the experiment, at both the neutral and the proton-transferred geometry.

3.2. Dimers. ***3.2.1. Ground-State Geometry.*** The structures of $(H_2O)_2^+$ considered in this work are shown in Figure 2. The neutral structure has C_s symmetry with the oxygen atoms separated by 2.91 Å. This geometry is not a stationary point on the cation PES and provides time-zero reference for the structure prepared by time-resolved spectroscopy. We refer to it as the vertical geometry. IEs and MOs at this geometry are shown in Figure 3. EOM-IP-CCSD and EOM-IP-CC(2,3) predict the vertical IE to be 11.4 and 11.3 eV, respectively. This is lower than the experimental value of 12.1 eV,[18] assuming that the absorption maximum in the recorded spectrum corresponds to a vertical transition, which depends on the population of different conformers in the experiment. The adiabatic IE was determined experimentally to lie in the range 10.8−11.2 eV.[16–18] The equivalent energy gap (not including zero-point energy differences) computed using EOM-IP-CCSD and EOM-IP-CC(2,3) is 10.55 and 10.40 eV, respectively.

Ionization facilitates the downhill barrierless proton transfer from the H-bond donor to the acceptor, leading to the formation of $OH \cdots H_3O^+$ (Figure 2b). Electronically, these products correlate with the $OH \cdots H_3O^+$ state of the neutral. There is a large geometric change associated with the proton transfer as the oxygen−oxygen distance decreases to 2.47 Å and the symmetry is lowered to C_1, due to an out-of-plane rotation of the OH fragment by 40°. However, the C_1 structure is lower by only 0.1 kcal/mol relative to the C_s proton-transferred configuration. In the C_s symmetry saddle, the oxygen−oxygen distance is also 2.47 Å.

To benchmark the DFT methods, we have investigated how different models reproduce the relative energies of the isomers. In view of SIE, we also included the hemibonded structure predicted to be the lowest isomer by some DFT calculations (Table 4). It has (near) C_{2h} symmetry with the charge distributed equally between the fragments. Such systems are problematic for both HF and DFT methods. The former tends to destabilize them because of symmetry breaking, whereas the latter overstabilize them because of SIE. The EOM-IP-CC methods based on the neutral reference are free from these artifacts. Table 3 compares the energies of the $(H_2O)_2^+$ isomers obtained at different levels of theory using wave function methods. These methods consistently predict the proton-transferred isomer to be lower than the hemibonded form. At the HF level, the difference between the proton-transferred and hemibonded

TABLE 1: Ionization Energies (eV) of H_2O, OH^-, and H_3O^+

	EOM-IP-CCSD		EOM-IP-CC(2,3)		
	6-311++G**	aug-cc-pVTZ	6-311++G**	aug-cc-pVTZ	exp
			H_2O		
$1b_1$	12.32	12.61	12.29	12.51	12.6,[a] 12.62[b]
$3a_1$	14.61	14.87	14.57	14.78	14.8,[a] 14.64[b]
$1b_2$	18.84	18.94	18.78	18.83	18.6,[a] 18.6[b]
			OH^-		
π	1.37	1.77	1.17	1.48	1.83[c]
σ	5.60	5.90	5.37	5.59	
			H_3O^+		
a_1	24.38	24.64	24.41	24.61	
e	30.16	30.25	30.17	30.21	

[a] Reference 66. [b] Reference 67. [c] References 68 and 69.

TABLE 2: Excitation Energies (eV) and Transition Properties (au) of H_2O^+, OH, and H_3O^{2+} (a 6-311++G Basis Set was Used Throughout)**

	EOM-IP-CCSD			EOM-EE-CCSD			EOM-IP-CC(2,3)	expt
	E_{ex}	μ^2	f	E_{ex}	μ^2	f	E_{ex}	E_{ex}
				H_2O^+ at the geometry of the neutral				
$3a_1-1b_1$	2.29	0.0229	0.00128	2.29	0.0225	0.00126	2.28	2.02[a]
$1b_2-1b_1$	6.52			6.48			6.49	6.0[a]
				H_2O^+ at the geometry of the cation				
$3a_1-1b_1$	2.02	0.0179	0.000885	2.01	0.0177	0.000874	2.01	1.89[b]
$1b_2-1b_1$	6.53			6.89			6.49 -	
				OH at the geometry of the neutral				
$\sigma-\pi$[a]	4.22	0.0301	0.00312	4.21	0.0311	0.00321	4.20	4.12[c]
				H_3O^{2+} at the geometry of H_3O^+				
a_1-e[b]	5.78	6.7×10^{-6}	9.5×10^{-7}	5.74	2.5×10^{-5}	3.4×10^{-6}	5.75	

[a] Computed as a difference of vertical IEs from ref 67. [b] Reference 70. [c] Reference 71.

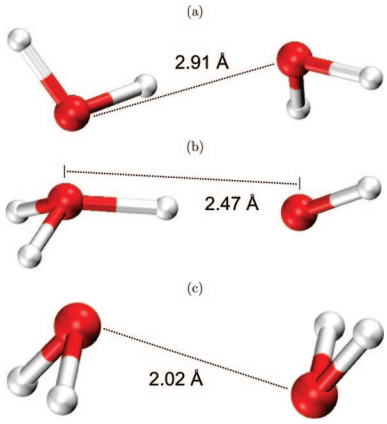

Figure 2. Geometries of (a) vertical neutral $(H_2O)_2$, (b) proton-transferred $(H_2O)_2^+$, and (c) hemibonded$(H_2O)_2^+$. Oxygen−oxygen distance has been marked on the plots.

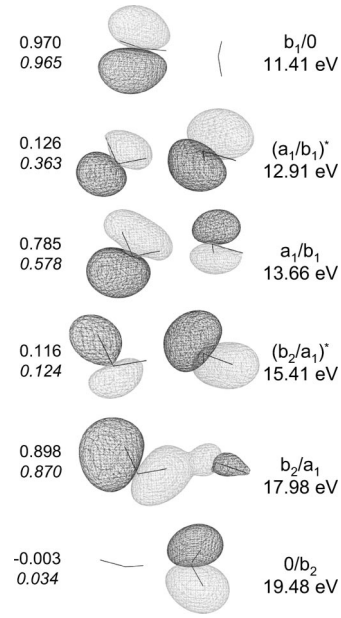

Figure 3. Six highest-occupied MOs of the neutral water dimer. Ionization energies were calculated using EOM-IP-CCSD/6-311++G**. The numbers on the left are the NBO charge on the H-bond donor fragment calculated using EOM-IP-CCSD (upper number) and CCSD/EOM-EE-CCSD (lower number) wave functions. The geometric frame is rotated for each orbital to best show orbital character. The NBO analysis of the reference CCSD/6-311++G** wave function showed a −0.012 charge on the H-bond donor.

structures is 26 kcal/mol, and electron correlation brings it down to 7−8 kcal/mol. The large difference at the HF level is due to the symmetry-breaking problem at the hemibonded geometry. The energy difference between the proton-transferred and vertical configurations only weakly depends on the level of theory and is approximately 20 kcal/mol. This stable behavior is due to the charge-localized character of the wave functions, which are free from the HF instability, and are described well using both open-shell and closed-shell references.

The set of $(H_2O)_2^+$ structures was re-optimized using DFT. The results are summarized in Table 4. The DFT calculations without SIC show the following trends. First, there is virtually no energy difference between the unrestricted and restricted open-shell BLYP results. Second, compared to the benchmark EOM-IP-CCSD calculations, BLYP overstabilizes both the

TABLE 3: Energies (kcal/mol) of $(H_2O)_2^+$ Relative to the Proton-Transferred Geometry Calculated Using Wave-Function-Based Methods (a 6-311++G Basis Set Was Used Throughout)**

	hemibonded	vertical neutral
HF	26.8	20.1
MP2	7.4	21.4
CCSD	9.9	21.4
CCSD(T)	8.2	21.6
EOM-IP-CCSD	5.3	20.0
EOM-IP-CC(2,3)	7.4	21.8

TABLE 4: Energies (kcal/mol) of $(H_2O)_2^+$ Relative to the Proton-Transferred Geometry Calculated Using DFT Methods

	hemibonded	vertical neutral
EOM-IP-CCSD geometry		
UBLYP/DZVP	−8.3	6.7
ROBLYP/DZVP	−8.3	6.6
SIC(0.2/0.0)−ROBLYP/DZVP	7.3	21.1
SIC(0.2/0.0)−ROBLYP/TZVDD	6.6	19.9
SIC(0.2/0.2)−ROBLYP/DZVP	1.0	15.0
optimized geometry		
UBLYP/DZVP	−8.8	
ROBLYP/DZVP	−8.7	
SIC(0.2/0.0)−ROBLYP/DZVP	7.7	
SIC(0.2/0.0)−ROBLYP/TZVDD	8.0	
SIC(0.2/0.2)−ROBLYP/DZVP	0.8	

vertical and the hemibonded dimer structures by −12 and −13 kcal/mol, respectively. The error for the hemibonded structure is comparable in absolute value to that of HF. However, the sign is opposite and, as was shown before,[28] the SIE uncorrected DFT erroneously places the hemibonded minimum below the proton-transferred one. This is a well-known signature of SIE observed in many systems with charge separation.[47,52,53]

A simple empirical SIC correction for doublet states based on removing SI of the unpaired electron implemented for restricted open-shell BLYP[48,49] improves the results significantly. For the recommended choice of the two scaling parameters (0.2 and 0), the error in the above relative energies drops to 2−3 kcal/mol (compared to EOM-IP-CCSD) and is further reduced to less than 2 kcal/mol upon moving from DZVP to TZVDD basis set. This is encouraging and justifies considering the use of DFT/BLYP with the present SIC for condensed-phase AIMD calculations.[12] Although it is theoretically more appealing to employ the same value for both scaling parameters (i.e., 0.2 and 0.2, as in other approaches[54]), this produces less-accurate results: the correct order of minima is still preserved, but the error increases to about −4 kcal/mol.

Finally, DFT re-optimization of the proton-transfer and hemibonded structures results in minor geometry and, consequently, minor energy changes (Table 4). The geometry of the neutral dimer, which is not a minimum on the cationic surface, collapses to the proton-transfer minimum upon minimization (as for EOM-IP-CCSD).

The use of restricted open-shell formalism with Kohn−Sham DFT deserves an additional comment. As shown by Pople and coworkers,[55] in open-shell systems that have excess α electrons, regions of negative spin density exist. That means that the local density of β electrons may be higher than the density of α electrons. The local excess of β electrons is reproduced by correlated calculations, as well as confirmed experimentally. In the DFT framework, it can only be reproduced within UKS formalism, simply because the electron density is a sum of the MO densities, which are the same for both spins in ROKS. However, the SIC applied here is stable only within ROKS formalism because it requires one to identify the unpaired electron. Density functionals containing non-local operators, such as long-range Hartree−Fock exchange, reduce the SIE in a more fundamental way.[56–60] However, symmetric radical cations are particularly difficult systems, and performance is not yet fully satisfactory.[60]

3.2.2. DMO-LCFMO Framework. The dimer spectroscopy can be explained in terms of the individual fragment contributions. The theoretical framework is provided by the DMO-LCFMO theory, which was applied previously to the electronic structure of the benzene dimer cation[15] and is described in the Appendix. It allows one to correlate the dimer and monomer transitions based on the degree of mixing of the FMOs in the dimer. We employ a (H-bond donor orbital)/(H-bond acceptor orbital) notation, allowing one to quickly discern the FMOs that contribute to a given DMO. If there is no component on the given fragment, then the symbol 0 is used. An asterisk signifies antibonding character of the dimer MO with respect to the fragment's interaction. The extent to which a given FMO participates in a given DMO can be quantified using the NBO analysis. NBO yields the charges of the fragments, which are related to the square of the diabatic wave function defined here as the charge-localized state. Below we discuss the DMOs at the vertical and at the proton-transferred geometry.

The orbitals at the vertical configuration are shown in Figure 3. The SOMO is the b_1 orbital of the H-bond donor molecule and is called $b_1/0$. It is antisymmetric with respect to the plane of symmetry. The delocalization of this orbital requires mixing with an antisymmetric orbital of the H-bond acceptor molecule. The only such orbital is $0/b_2$, which is high in energy, and, therefore, the ground state hole is localized. The two lower orbitals are linear combinations of the acceptor b_1 and the donor a_1 MOs. The higher energy combination is antibonding with respect to the monomers and is called $(a_1/b_1)^*$. The bonding combination is (a_1/b_1). Lower in energy, we find the $(b_2/a_1)^*$ and (b_2/a_1) pair. The antibonding DMO is located mostly on the acceptor, whereas the donor hosts the bonding component. Finally, the acceptor $0/b_2$ is the lowest DMO considered here. States corresponding to ionizing the H-bond donor are lower in energy (the corresponding FMOs are higher in energy), which can be rationalized easily in terms of electrostatic interaction. A hole on the H-bond donor fragment is stabilized by the negatively charged oxygen of the acceptor, whereas a hole on the acceptor is destabilized by the positively charged proton.

Orbitals at the C_s and C_1 proton-transferred configurations are shown in Figure 4. The proton transfer changes the character of the MOs drastically, and it is no longer possible to diabatically correlate them with those of the neutral. The MOs clearly separate into the H_3O^+ and OH fragments. Orbitals of the hydroxyl part are higher in energy than those of H_3O^+, as follows from the difference of IEs. Under C_s symmetry, the HOMO is the out-of-plane component of the degenerate π-pair on the OH^- fragment, $\pi_{oop}/0$. Below it are the $\pi_{inp}/0$ and $\sigma/0$ DMOs. The degenerate π system follows the out-of-plane rotation of the hydroxyl group. H_3O^+ orbitals appear in the following order: $0/a_1$, 0/e', and 0/e". The OH σ and H_3O^+ e' orbitals are slightly mixed. Overall, only minor differences are observed in the C_s and C_1 structure orbitals.

The NBO charges reveal stronger delocalization than suggested by visual inspection of the MOs. The delocalization is due the wave function having significant amplitude between the two fragments at close distances. Additionally, for the excitations

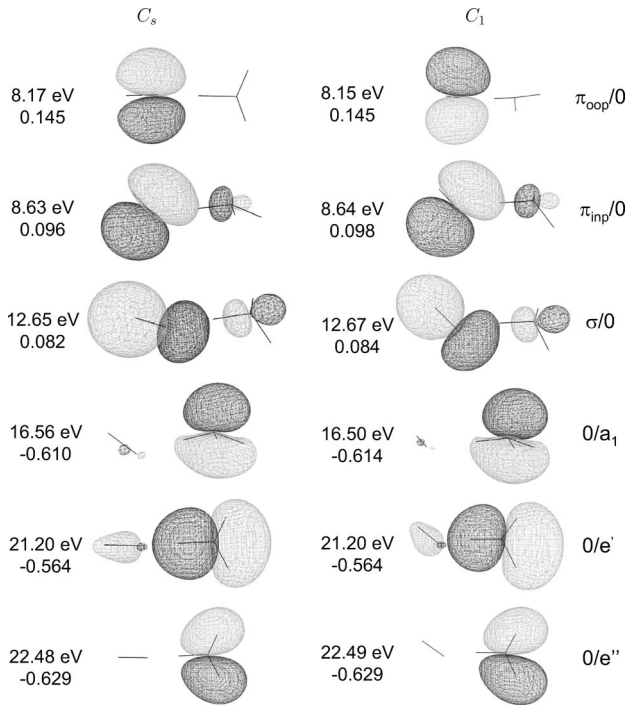

Figure 4. Six highest-occupied MOs of the neutral water dimer at the C_s and C_1 proton-transferred configurations. Ionization energies were calculated using EOM-IP-CCSD/6-311++G**. The NBO charge on the hydroxyl radical calculated using EOM-IP-CCSD wave functions is given below. The geometric frame is rotated for each orbital to best show orbital character. The NBO analysis of the reference CCSD/6-311++G** wave function showed −0.771 and −0.770 charge on the hydroxyl radical in the C_s and C_1 structures, respectively.

from H_3O^+ to OH one might expect to see a −1 charge on the hydroxyl fragment. However, the large positive charge on H_3O^{2+} will polarize the OH^- and thus decrease its charge. This is confirmed by the calculation, revealing −0.771 charge on the OH moiety.

3.2.3. Spectroscopy at the Vertical Configuration. Table 5 and Figure 5 present excitation energies and transition properties of $(H_2O)_2^+$ at the geometry of the neutral species. All excitations involve transfer of an electron to the SOMO, that is, the $b_1/0$ orbital. Overall, all theoretical methods are in good agreement in terms of energetics. A state involving excitation to a virtual orbital of the neutral appeared in the EOM-EE-CCSD calculation at 8 eV and was disregarded.

At low energies, up to ca. 2 eV, we find excitations from the $(a_1/b_1)^*$ and (a_1/b_1) pair into the SOMO. Their intensity can originate from both the intramolecular and intermolecular terms and reflects the partitioning of the DMOs into FMOs, and can be explained by DMO-LCFMO. Referring to the formalism summarized in the Appendix, $(a_1/b_1)^*$ and (a_1/b_1) are examples of DMOs in which both the α and β coefficients (i.e., the weights of the FMOs) are significant. The weights of the FMOs are just the square roots of the EOM-IP-CCSD NBO charges because both fragments are neutral in the reference state:

$$(a_1/b_1)^* = 0.355(a_1/0) - 0.935(0/b_1) \quad (3)$$

$$(a_1/b_1) = 0.886(a_1/0) + 0.464(0/b_1) \quad (4)$$

Neglecting the intermolecular contribution to the intensity, one can evaluate the transition dipole moments for the two transitions according to eq 7. The corresponding squares are 0.0029 and 0.0180 au^2. This estimate is in excellent agreement with the actual EOM-IP-CCSD dimer calculation, which yields 0.0038 and 0.0181 au^2, thus supporting the assumption that these two transitions draw their intensity from the H-bond donor a_1 component of the DMO and that the intermolecular terms are negligible. The EOM-IP-CCSD and EOM-EE-CCSD methods predict different relative intensity of the two bands. Although EOM-EE-CCSD predicts nearly equal intensities, EOM-IP-CCSD suggests a 1:5 intensity ratio in favor of the higher energy band. The origins of this discrepancy can be traced back to different partitioning of the a_1 component between the $(a_1/b_1)^*$ and (a_1/b_1) pair. Our benchmark study[61] demonstrated that EOM-IP-CCSD provides a more accurate description of charge delocalization and more accurate transition properties.

EOM-IP-CCSD predicts weak excitations from the $(b_2/a_1)^*$ and (b_2/a_1) pair to be at 4 and 6.5 eV, respectively. EOM-EE-CCSD predicts the transition from the antibonding DMO to lie 0.3 eV higher and agrees as to the position of transition from the bonding DMO. The antibonding orbital is confined to the H-bond acceptor, while the bonding orbital is confined to the donor. Conceptually, the character of the transitions is similar to that discussed above. These two excitations correspond to the symmetry-forbidden $b_1 \leftarrow a_1$ excitation in the monomer. Consequently, the intramolecular term in eq 7 is zero. Orbital relaxation and intermolecular terms account for the intensity of these bands, which are still 100 times weaker than the allowed transitions.

Finally, around 8 eV we find the $(b_1/0) \leftarrow (0/b_2)$ transition. It is a pure charge-transfer band ($\alpha = 0$), where the hole is moved from the donor to the acceptor molecule. Its considerable intensity is due to particularly favorable overlap between the initial and final orbitals. The transition is still one order of magnitude weaker than the sum of the $(b_1/0) \leftarrow (a_1/b_1)$ and $(b_1/0) \leftarrow (a_1/b_1)^*$ excitations.

3.2.4. Spectroscopic Signatures of Proton Transfer. Excitation energies and transition properties at the C_1 and C_s proton-transferred geometries are presented in Tables 6 and 7, respectively. The EOM-IP-CCSD data are shown in Figure 6. We were able to obtain EOM-EE-CCSD results only for the three lowest excitations because the states involving virtual orbitals of the neutral wave function are the next higher in energy. The lowest-energy transition is at 9.6 eV, well beyond the energy range potentially probed in a pump-probe experiment. Additionally, the Rydberg character of these states means that they are likely to be significantly perturbed in the condensed phase. All of the excitations considered here involve the transfer of an electron to the singly occupied $(\pi_{oop}/0)$ orbital. Because of the localized character of the DMOs, the spectrum partitions into two parts: transitions within the OH fragment and transitions from the H_3O^+ to the OH fragment. In the language of the Appendix, the lower-energy part of the spectrum is close to the $\beta = 0$ limit, whereas the higher energy one approaches the $\alpha = 0$ limit, that is, local and charge-transfer excitations, respectively.

The C_s and C_1 configurations differ only slightly in positions and intensities of the transitions in the low-energy part of the spectrum. The transitions in this region are from the $(\pi_{inp}/0)$ and $(\sigma/0)$ orbitals. The former excitation is not present in an isolated OH monomer, as the $(\pi_{inp}/0) - (\pi_{oop}/0)$ pair is degenerate. In the dimer, it splits by 0.5 eV and acquires oscillator strength. The $(\pi_{oop}/0) \leftarrow (\sigma/0)$ excitation is at 4.5 eV, very close to the monomer value of 4.2 eV; however, its intensity is less than half. The origin of the intensity decrease can be investigated using DMO-LCFMO, although its quantitative application is complicated by the large extent of charge transfer occurring in the neutral and in the cation states. We

TABLE 5: Excitation Energies (eV) and Transition Properties (au) of the $(H_2O)_2^+$ Cation at the Geometry of the Neutral (All Transitions Are to the 2a″ (b_1/0) Orbital, and a 6-311++G Basis Set Was Used Throughout)**

		EOM-IP-CCSD			EOM-EE-CCSD			EOM-IP-CC(2,3)
		E_{ex}	μ^2	f	E_{ex}	μ^2	f	E_{ex}
8a′	$(a_1/b_1)^*$	1.50	0.00379	1.39×10^{-4}	1.81	0.00995	4.41×10^{-4}	1.48
7a′	a_1/b_1	2.25	0.0181	9.98×10^{-4}	2.37	0.0122	7.06×10^{-4}	2.23
6a′	$(b_2/a_1)^*$	3.99	6.95×10^{-4}	6.80×10^{-5}	4.34	$1.69\ 10^{-4}$	1.80×10^{-5}	3.97
5a′	b_2/a_1	6.57	7.29×10^{-6}	1.12×10^{-6}	6.56	$1.65\ 10^{-5}$	2.65×10^{-6}	6.52
1a″	$0/b_2$	8.07	0.00362	7.16×10^{-4}	8.46	0.00183	3.80×10^{-4}	8.04

TABLE 6: Excitation Energies (eV) and Transition Properties (au) of the $(H_2O)_2^+$ Cation at the C_1 Proton-Transferred Geometry (All Transitions Are to the $10a_1$ (π_{oop} /0) Orbital, and a 6-311++G Basis Set Was Used Throughout)**

		EOM-IP-CCSD			EOM-EE-CCSD		
		E_{ex}	μ^2	f	E_{ex}	μ^2	f
$9a_1$	π_{inp}/0	0.49	0.00190	2.28×10^{-5}	0.49	0.00220	2.66×10^{-5}
$8a_1$	σ/0	4.52	0.0136	0.00151	4.53	0.0129	0.00143
$7a_1$	$0/a_1$	8.35	0.0141	0.00289	8.87	0.00957	0.00208
$6a_1$	0/e'	13.05	0.00194	6.21×10^{-4}			
$5a_1$	0/e"	14.34	0.00224	7.86×10^{-4}			

TABLE 7: Excitation Energies (eV) and Transition Properties (au) of the $(H_2\ O)_2^+$ Cation at the C_s Proton-Transferred Geometry (All Transitions Are to the $10a_1$ (π_{oop}/0) Orbital, and a 6-311++G Basis Set Was Used Throughout)**

		EOM-IP-CCSD			EOM-EE-CCSD		
		E_{ex}	μ^2	f	E_{ex}	μ^2	f
8a′	π_{oop}/0	0.46	0.00176	$2.01\ 10^{-5}$	0.50	0.00217	$2.50\ 10^{-5}$
7a′	σ/0	4.48	0.0138	0.00151	4.49	0.0132	0.00145
6a′	$0/a_1$	8.39	$3.11\ 10^{-5}$	$6.40\ 10^{-6}$	8.95	$1.13\ 10^{-5}$	$2.47\ 10^{-6}$
5a′	$0/e'$	13.03	$7.07\ 10^{-4}$	$2.26\ 10^{-4}$			
4a″	0/e″	14.31	0.00593	0.00208			

discuss the calculation for the C_s structure, but the result for the C_1 geometry is essentially identical. To obtain the singly occupied orbital, one needs to consider the difference between the neutral and the cation states (the singly occupied orbital is the same as the orbital of the outgoing electron). The NBO analysis of the CCSD wave function of the $OH^-\cdots H_3O^+$ system revealed a −0.771 charge on the hydroxyl moiety. In other words, 0.916 and 0.853 electrons come from this moiety when an electron is removed from the (π_{inp}/0) and (σ/0) orbitals, respectively. Using these numbers to calculate the weights of the appropriate diabatic states and, subsequently, the transition dipole moment, one obtains 0.024 au,[2] almost twice the ab initio calculated value. The source of the discrepancy appears to be the coupling with 0/e′ and the arising intermolecular contribution to the intensity.

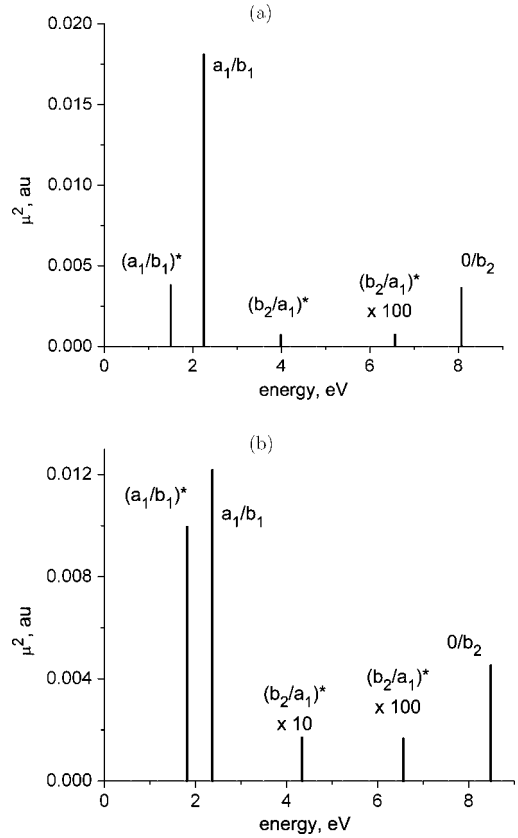

Figure 5. Electronic state's ordering and transition dipole moments of water dimer cation at the neutral configuration calculated using (a) EOM-IP-CCSD/6-311++G** and (b) EOM-EE-CCSD/6-311++G**. All transitions are to the b_1/0 orbital.

Higher in energy, there are excitations involving the transfer of an electron from H_3O^+ to OH. The first one, at ∼8 eV, is the transition from the lone-pair ($0/a_1$) orbital. It is very weak in the C_s structure; however, upon rotation of the hydroxyl group it acquires intensity comparable to the (π_{oop}/0) ← (σ/0) transition, presumably because of the favorable overlap of the two DMOs, which increases upon rotation. In the C_s structure, the two orbitals resemble two orthogonal p orbitals. Hence, the positive and negative contributions to the transition dipole moment cancel out. In C_1, they are akin to p_z orbitals form the π system in ethylene and all the contributions have the same sign. Above 13 eV, we find excitations from (0/e′) and (0/e″).

3.2.5. Proton-Transfer PES Scan. Figure 7a presents the PES scan of the proton-transfer reaction in the C_s geometry. The coordinates are the oxygen−oxygen distance and the distance between the transferring proton and the accepting oxygen. Points A and C correspond to the vertical and proton-transferred geometries, respectively. They were identified based solely on the two geometric parameters scanned. The energy of point A is 3.5 kcal/mol lower than the energy at the neutral geometry because of relaxation of unconstrained coordinates. This lowers the energy change due to the reaction from 20 to 16.5 kcal/mol. A two-step picture of the proton-transfer reaction emerges from the graph. Between points A and B, the H-bond donor molecule moves towards the acceptor, as the oxygen−oxygen and hydrogen−oxygen distances change in unison. This motion lowers the energy by 11.4 kcal/mol. Subsequent dynamics is restricted to the proton, which transfers from the donor to the acceptor, accompanied by minor adjustments in the oxygen−oxygen distance. An energy change of 5.0 kcal/mol is associated with this motion.

The PES allows us to compute the spectral changes along the steepest descent reaction path. Calculated excitation energies

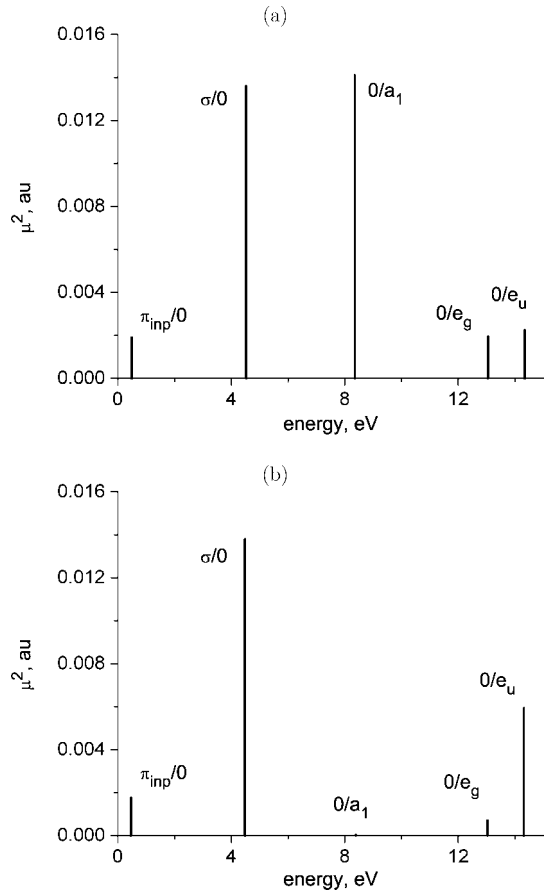

Figure 6. Electronic states ordering and transition dipole moments of the water dimer cation at the C_1 (a) and C_s symmetry proton-transferred configurations calculated using EOM-IP-CCSD/6-311++G**. All transitions are to the $\pi_{oop}/0$ orbital.

and transition properties are presented in Figure 7b and d. We employ the C_s symmetry labels to identify the states in this discussion, as the character of the orbitals changes along the reaction coordinate. All of the transitions involve the transfer of an electron to SOMO, the 2a″ orbital, which is the out-of-plane orbital on the H-bond donor. Its character evolves from the H_2O^+ lone-pair b_1 orbital to the π orbital of OH. Of particular interest are the 6a′, 7a′, and 8a′ transitions because they are within the spectroscopic 1−6 eV window. At point A, two absorption bands appear around 2 eV (8a′ and 7a′). They are transitions from the bonding and antibonding combinations of the donor a_1 and acceptor b_1 fragment MOs [$(a_1/b_1)^*$ and (a_1/b_1)]. The lower-energy transition carries more intensity, which is different from the fully optimized neutral configuration, where the higher energy transition carries more intensity. This is due to the slightly different geometry and orbital mixing of the H-bond acceptor b_1 and donor a_1 in the two states. 6a′ and 5a′ are bonding and antibonding combinations of donor b_2 and acceptor a_1. They are at 6.2 and 4.3 eV, respectively. The intensities of both bands are small. Finally, at 8.5 eV we find the transition from the 1a″ (acceptor b_2) orbital.

As the reaction proceeds to point B, the intensity of 8a′ and 7a′ changes as the bands move apart. In other words, the partitioning of H-bond donor a_1 and acceptor b_1 in the $(a_1/b_1)^*$ and (a_1/b_1) pair changes. The small-magnitude of change is understood easily within the diabatic framework of $(a_1/0)$ and $(0/b_1)$ states, that is, the states with the charge localized on the H-bond donor and acceptor, respectively. The coupling and separation of the diabatic states increase at shorter distances. The two effects largely cancel out, and no drastic changes in intensity are observed. There is a small increase in the intensity of the 6a′ (H-bond acceptor a_1) band.

At point B, the proton-transfer step starts taking place and the character of MOs changes more dramatically. The SOMO becomes the out-of-plane π orbital. The intensity of the 8a′ band drops significantly with a decrease in energy as it becomes a $\pi-\pi$ transition on the OH fragment. The 7a′ excitation gains intensity as the energy rises to 4.5 eV and becomes the $\sigma-\pi$ excitation. At the same time, the 6a′ and 5a′ excitations move to higher energy, becoming CT excitations from H_3O^+ to OH. The already small intensity of excitation from 6a′ drops further as it becomes the apical orbital of H_3O^+. Both 1a″ and 5a′ transitions move to 12−14 eV, outside the experimental region.

4. Discussion

Three geometries on the ground-state PES of the water dimer cation are of prime importance in the photoionization process. The first two are minima: the proton-transferred and the hemibonded structures (Figure 2b and c). The third one is the geometry of the neutral dimer reached by vertical ionization (Figure 2a). The geometries and relative energetics of these structures calculated by correlated electronic structure methods are in good agreement with each other (Table 3) and previous ab initio results.[24,25,28] All of these calculation correctly characterize the proton-transferred geometry as the global minimum lying 5−10 kcal/mol below the hemibonded local minimum and about 20 kcal/mol below the structure corresponding to vertical ionization of the neutral water dimer. This ordering is reproduced already at the HF level, which, however, grossly (by about 20 kcal/mol) destabilizes the hemibonded structure due to the tendency of HF to artificially localize the MOs in systems with symmetrically equivalent centers. In contrast, the proton-transferred structure has spin-localized on one fragment and charge-localized on the other; and in the vertical geometry, corresponding to the neutral water dimer, the spin and charge are initially localized on one water. The behavior of the DFT methods is exactly opposite. Because of SIE, DFT/BLYP overstabilizes structures with delocalized charge and erroneously predicts the hemibonded structure to be the global minimum. However, a simple empirical a posteriori SIC[48,49] almost completely removes this artifact; and the predictions of the SIC-corrected DFT methods are very close to those of MP2. This is good news for the DFT-based AIMD studies of ionization in liquid water.[12] Nonetheless, further benchmark studies including the spin localization and cluster dynamics are needed.

For ionization in the condensed phase, the issue of electronic localization/delocalization is of interest. We are interested in the question of whether the charge is localized at one site immediately upon ionization or whether it will localize after being initially delocalized over many water molecules. This localization process can be explored only by considering clusters beyond the dimer. In the dimer, the hole forms on the b_1 orbital of the H-donor fragment immediately upon ionization. This initial localization is due to the fact that the donor water is not acting as an acceptor to any other H bond. The b_1 orbital of the H-bond acceptor in fact couples with the a_1 orbital of the donor. The neutral water dimer thus represents the most asymmetric arrangement of water molecules. Already in the cyclic trimer, the water molecules become equivalent, which means that upon ionization the hole must be initially delocalized. In the bulk phase, each water molecule is likely to serve as a hydrogen-bond acceptor and donor simultaneously, thus more likely delocalizing the hole. However, in the initial period of delo-

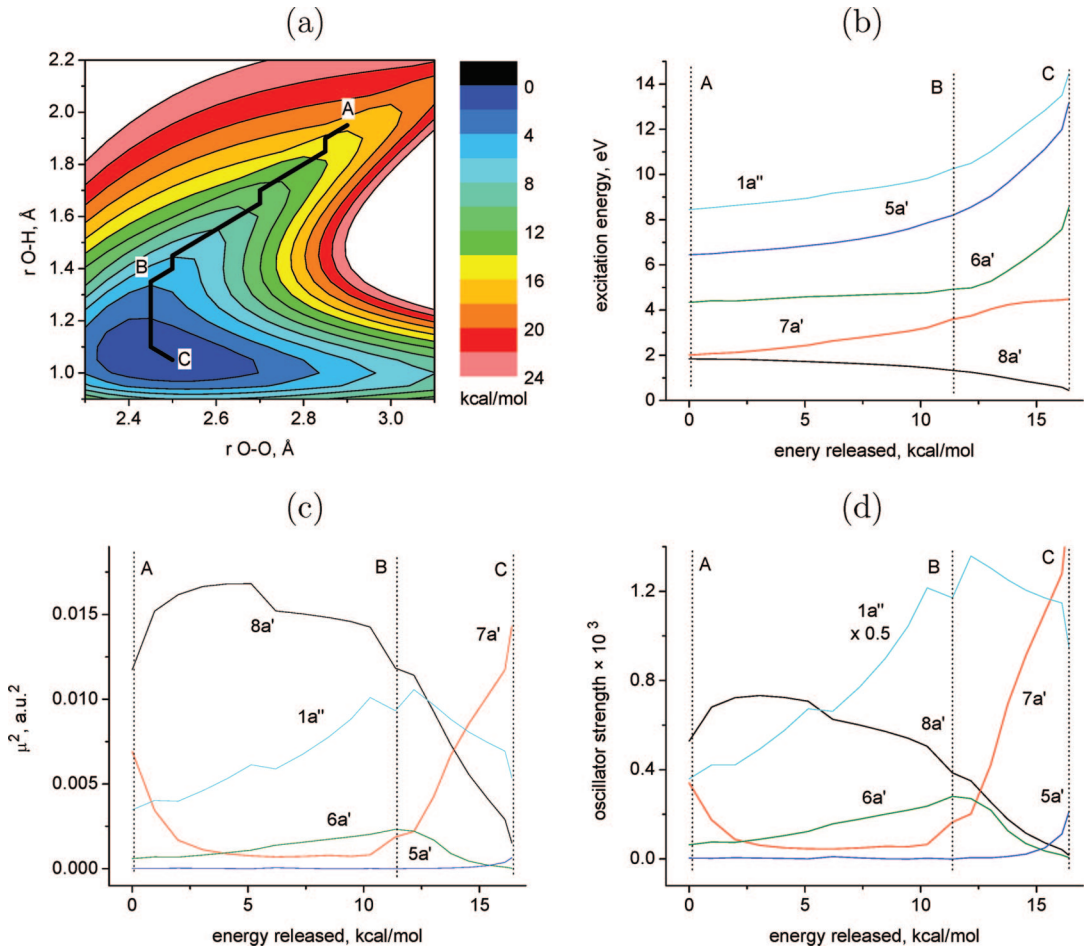

Figure 7. (a) The ground-state PES scan for the proton-transfer reaction. The *x*-axis is the oxygen−oxygen distance, and the *y*-axis is the distance between the transferring proton and the accepting oxygen. At each point, a constrained geometry optimization was conducted. Points A and C correspond to the neutral and proton transferred geometries, respectively. Point B marks the start of the proton transfer. The black line is the steepest descent path. (b−d) Vertical excitation energies, transition dipole moments, and oscillator strengths along the reaction coordinate. All calculations were done using EOM-IP-CCSD/6-311++G**.

calization, which is not yet known, the positive charge will localize, thereby starting the proton-transfer reaction. From this point onward, the dimer is presumably an adequate model for the spectroscopy of the condensed-phase proton-transfer process.

In general, small- and medium-sized water clusters with different geometries will provide a natural laboratory to investigate the electronic and nuclear dynamics upon ionization with varying degrees of initial localization/delocalization of the hole.[62]

Charge localization is intimately related to the electronic spectroscopy of the system. Using formalism of the Appendix, both the α and β coefficients may be significant (delocalized charge), or one can dominate (localized). Thus, excitations will have a mixed charge transfer and local character. With no knowledge of the degree of charge delocalization, it is impossible to say anything about the intensity of mixed bands and reliable ab initio calculations are needed. In the case of dimer cation states, one may expect intermolecular contributions to be less significant than those in their neutral counterparts because of the more-compact nature of MOs. This maybe counteracted by the decreased separation manifested in a charged species. Our calculations for the water dimer cation reveal that the intermolecular terms are typically one order of magnitude smaller than the intramolecular terms for allowed transitions. Note, however, that the interfragment contribution varies exponentially with the distance (separately from α and β) and may change significantly with relative orientation of the two fragments, thus allowing one to monitor the molecular dynamics via intensity and/or position of those bands.

Next, we discuss the nuclear motions along the reaction coordinate leading from the geometry corresponding to the neutral water dimer to the proton-transfer structure (Figure 7a). The reaction, which is a downhill process without a barrier, proceeds in two steps. The first one involves heavy atom motions; that is, the two water molecules move closer to each other with the oxygen−oxygen distance decreasing from 2.9 to 2.5 A. This step is responsible for the largest part of the energy gain (~12 kcal/mol) along the reaction coordinate. Because it involves the motion of heavy atoms, it is relatively slow compared to the second step, the rapid transfer of the proton, which can happen only when the water oxygens are sufficiently close to each other. This process involves a motion of a light particle and is, therefore, possibly as fast as a few femtoseconds. Precise time scales are under detailed experimental and theoretical investigation in our labs. The energy gain associated with the proton hop is smaller, amounting to roughly 5 kcal/mol. In larger clusters and in bulk liquid water, this two-step mechanism should be preserved, although it might be preceded by initial fast charge localization.[12] This is exactly the dynamics that we wish to resolve in the condensed phase, with a spectroscopic

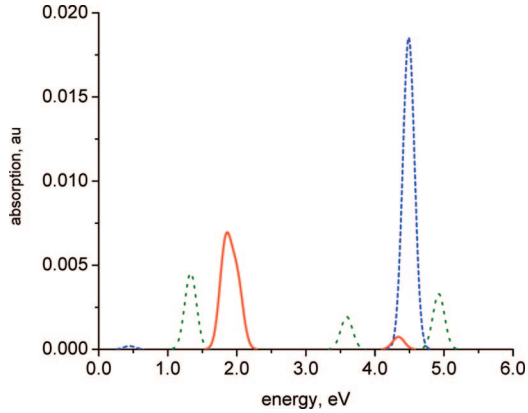

Figure 8. Evolution of the electronic spectrum of the water dimer cation along the reaction path at points A (red solid line), B (green dotted line), and C (blue dashed line). Points A and C correspond to vertical neutral and proton-transferred geometries. Point B marks the start of the proton transfer. 0.2 eV full width at half-maximum was assumed. See Figure 7 for details.

handle on these events being provided by the changing excitation spectrum of the radical species along the proton-transfer reaction.

Let us consider how the electronic transitions, their band positions, and their intensities evolve as we move along the reaction coordinate. Femtosecond spectroscopy should be able to monitor the system evolution by recording the changing transient absorption spectrum. Formally, the H_2O^+ cation is derived from the OH radical by the addition of a proton. One might thus expect the electronic structure and the spectroscopy of the two species to be similar. However, the results from Table 2 show that the addition of a proton is not a benign perturbation to the electronic structure. The OH radical has a characteristic absorption band around 4.2 eV corresponding to the transition of the bonding σ electron into the nonbonding π hole. Even if the proton is brought up along the O−H axis leading to a linear $H-O-H^+$, then the σ to π promotion is pushed up to higher energy (~6 eV). More significantly, allowing the structure to adopt the lower-energy bent configuration splits the π orbital into b_1 and a_1 symmetry components. The former $\pi \leftarrow \sigma$ transition becomes dipole-forbidden for the ground-state component ($b_1 \leftarrow b_2$). In C_{2v}, the transition between the two formerly degenerate b_1 and a_1 orbitals is dipole-allowed with a transition energy of ca. 2.3 eV and $^1/_3$ of the oscillator strength of the OH transition. Simply put, the 4-eV band disappears and a weaker 2.3-eV band appears in its place.

At the vertical geometry, the transitions for the ionized water dimer are perturbed and include some charge-transfer character; however, the wave functions can still be correlated with those of the monomers. Extracting the three points A, B, and C from Figure 7, we have replotted how the experimental spectrum can track the chemical reaction dynamics in Figure 8. At A, the bands at 2 eV ($b_1/0$) ← (a_1/b_1)* and ($b_1/0$) ← (a_1/b_1) [2a″ ← 8a′ and 2a″ ← 7a′] have almost the same oscillator strength as the monomer. The distribution of intensity between the two depends heavily on the system geometry. The 6-eV monomer-like transition is now not strictly symmetry-forbidden, particularly the 4-eV ($b_2/0$) ← (b_2/a_1)* [2a″ ← 6a′] component with more CT character. It still is almost two orders of magnitude weaker than the 2-eV transition. Therefore, the dominant characteristic electronic absorption of the dimer cation at the Franck−Condon geometry is around 2 eV (620 nm), as for the gas-phase monomer. Then at B, the ($b_2/0$) ← (a_1/b_1)* and ($b_2/0$) ← (a_1/b_1) [2a″ ← 8a′ and 2a″ ← 7a′] shift apart, the lower-energy band carrying more intensity. The 4-eV transition shifts slightly to the blue. At this point, proton-transfer begins. The lower-energy band becomes a weak $\pi-\pi$ excitation, while the 4-eV band gains intensity to become the $\sigma-\pi$ excitation. The shift is a clear fingerprint of the reaction, and the significant change corresponds to the charge-transfer between the species, that is, from B to C. Overall, the band positions resemble the monomers; however, the intensity pattern and fine structure are strong functions of the relative geometries in the cluster. For example, the comparison of the C_s and C_1 geometries of the proton-transferred complexes show a dramatic variation in the $0/a_1$ [6a′] band because of the alignment of the p orbitals on the two fragments. Although C_s is a saddle point between the two equivalent C_1 configurations of the product, it is only 0.1 kcal/mol above the minima and it allows us to symmetry-label the spectroscopic state of the evolving system. However, the transition to C_1 does lead to this large intensity change and one should be wary of the role of conformational changes in the band intensities.

We are now ready to discuss the effects of bulk water. Even if the dimer core is a good representation of the vertically prepared hole in water, then there is a large range of local neutral donor−acceptor geometries populated in room-temperature water. Although the configuration considered is the lowest-energy cluster, other configurations, particularly with different orientations of the free hydrogen of the donor with respect to the acceptor σ_v plane, should also be considered. Preliminary calculations have shown that if the O−H group of the H-bond donor is aligned with one of the acceptor O−H bonds (the donor molecule is rotated by ~90°), then the transitions with significant charge-transfer character can be enhanced significantly.[62] In particular, the band around 4 eV that involves CT ($b_2/0$) → (b_2/a_1)* [2a″ ← 7a′] acquires oscillator strength and can become comparable to the valence band near 2.3 eV. What if more solvating waters are included around the ionized core water? Preliminary EOM-IP-CCSD computations on a vertically ionized pentamer extracted from ice Ih show that excitations on a central water give rise to a spectrum similar to that of the monomer with an intense band near 2 eV and little oscillator strength at 4 eV. These results will be further quantified elsewhere.[62]

5. Conclusions

The water dimer cation is a prototypical system for the proton-transfer process in the gas and condensed phases. The vertical structure formed immediately upon ionization is not a stationary point on the cation PES, and the system follows the downhill gradient to $OH\cdots H_3O^+$. Our study demonstrates that this process can be monitored by femtosecond time-resolved electronic spectroscopy. At the simplest level, the initial spectrum resembles that of H_2O^+. As the reaction proceeds, band positions and intensities change. The product of the reaction spectroscopically resembles the free OH radical. A more detailed look at how the electronic spectrum evolves along the proton-transfer coordinate shows that changes in electronic structure are more subtle. We observed strong coupling between the H-bond donor and acceptor orbitals, which dissolves the monomer states into more delocalized dimer states. This coupling, which is likely to be present in the condensed phase as well, will lead to significantly delocalized states. Modeling of such states requires a full quantum treatment of the entire system. Hybrid quantum mechanical/molecular mechanical methods are not appropriate for this situation because the system cannot be partitioned into a solvent and a chromophore, as, for example, in our study of

electronic spectroscopy of the solvated CN radical.[63] AIMD, which is able to directly describe the electronic structure of the entire system, requires a fast electronic structure method, and presently DFT-based methods are the only viable choice. We have found that the energetics and structures of $(H_2O)_2^+$ are reproduced reasonably by the ROKS-BLYP method with the simple SIC correction,[48,49] which thus can be employed in AIMD simulations of the bulk.

Appendix

This section outlines the qualitative DMO-LCFMO framework for the description of the electronic states of the water dimer cation. This approach, rooted in the exciton theory,[64,65] was developed and applied to the electronic structure of the benzene dimer cation.[15] DMO-LCFMO describes the electronic wave functions of the dimer in terms of the dimer molecular orbitals expressed in the basis of the monomer MOs, which allows one to correlate properties of the dimer with the properties of the fragments. For the ionized dimers, one need not consider the full many-electron wave function of the initial and final states because they can be mapped onto 1-electron-in-2-orbitals ones. The two orbitals are the orbitals involved in the transition. In the cases considered in this work, the target orbital is always the same (SOMO of the cation).

An important feature distinguishing the benzene and water systems is greater charge localization in the ground state of $(H_2O)_2^+$. The SOMO is the out-of-plane p orbital of the hydrogen-bond donor, and all of the considered excitation are transfers of an electron to this orbital. In the 1-electron-in-2-orbitals picture this orbital is vacant, whereas the other one is singly occupied.

Let us introduce a basis of three localized fragment MOs: ω_A, ν_A, λ_B, where the subscript denotes the fragment. Because one of the states in $(H_2O)_2^+$ is localized, only a single basis function on fragment B is required. A similar approach is used in molecular electronic structure, where molecular states are described in terms of AOs. Recall, for example, $\sigma(2p_z)$ in O_2 or $\pi(p_y)$ and $\pi^*(p_y)$ in ethylene. In $(H_2O)_2^+$, we use the occupied orbitals of water monomer. We assume that the lower energy MO of the dimer is a delocalized mixture of ν_A and λ_B:

$$|\psi_1\rangle = \alpha|\nu_A\rangle + \beta|\lambda_B\rangle \quad (5)$$

where α and β satisfy the orthonormalization condition. The higher-energy DMO is the localized ω_A state:

$$|\psi_2\rangle = |\omega_A\rangle \quad (6)$$

This orbital represents the localized SOMO of $(H_2O)_2^+$. The transition takes place from $|\psi_1\rangle$ to $|\psi_2\rangle$. The transition dipole moment between states 1 and 2 is

$$\langle\psi_1|\hat{\mu}|\psi_2\rangle = \alpha\langle\nu_A|\hat{\mu}|\omega_A\rangle + \beta\langle\lambda_B|\hat{\mu}|\omega_A\rangle \quad (7)$$

The equation shows that both interfragment ($\langle\lambda_B|\hat{\mu}|\omega_A\rangle$) and intrafragment ($\langle\nu_A|\hat{\mu}|\omega_A\rangle$) terms contribute to the intensity of a dimer transition. The weight of each contribution is defined by the degree of MO mixing, that is, the α and β coefficients. Their relative phase determines whether individual contributions add or subtract. Thus, the total intensity of the monomer bands is not necessarily conserved in the dimer.

Consider first the limit of the ground state being completely localized on fragment B ($\alpha = 0$):

$$\langle\psi_1|\hat{\mu}|\psi_2\rangle = \langle\lambda_B|\hat{\mu}|\omega_A\rangle \quad (8)$$

The transition becomes a pure charge-transfer excitation in which the electron moves from B to A. Its intensity may become strong when the fragments are closer together but will decrease rapidly with the distance because of the exponential decay of the fragment wave functions. In the limit of the excited state localized on A ($\beta = 0$), we obtain

$$\langle\psi_1|\hat{\mu}|\psi_2\rangle = \langle\nu_A|\hat{\mu}|\omega_A\rangle \quad (9)$$

Thus, the excitation becomes a purely local excitation on fragment A. Within this framework, the electron density on fragment B is not affected. Its intensity is the same as that in the monomer; that is, a forbidden excitation remains forbidden and an allowed one remains allowed. However, in a dimer the orbitals and molecular geometries become distorted relative to isolated fragments and forbidden transitions often acquire small intensities.

Acknowledgment. We thank Dr. C.G. Elles for discussions and helpful comments. This work was conducted under the auspices of the *iOpenShell* Center for Computational Studies of Electronic Structure and Spectroscopy of Open-Shell and Electronically Excited Species (iopenshell.usc.edu) supported by the National Science Foundation through CRIF:CRF CHE-0625419+0624602+0625237 grant. J.V. acknowledges Prof. M. Sprik and Prof. J. Hutter for valuable discussions and support. P.J. acknowledges support from the Czech Ministry of Education (grant LC512) and the Granting Agency of the Czech Republic (grant 202/06/0286). S.E.B. gratefully acknowledges the support of the National Science Foundation through grant CHE-0617060.

7. Supporting Information Optimized molecular geometries. This material is available free of charge via the Internet at http://pubs.acs.org.

References and Notes

(1) Sancar, A. *Biochemistry* **1994**, *33*, 2.
(2) Bixon, M.; Jortner, J. *J. Phys. Chem. A* **2001**, *105*, 10322.
(3) Garrett, B.C.; Dixon, D.A.; Camaioni, D.M.; Chipman, D.M.; Johnson, M.A.; Jonah, C.D.; Kimmel, G.A.; Miller, J.H.; Rescigno, T.N.; Rossky, P.J.; Xantheas, S.S.; Colson, S.D.; Laufer, A.H.; Ray, D.; Barbara, P.F.; Bartels, D.M.; Becker, K.H.; Bowen, H.; Bradforth, S.E.; Carmichael, I.; Coe, J.V.; Corrales, L.R.; Cowin, J.P.; Dupuis, M.; Eisenthal, K.B.; Franz, J.A.; Gutowski, M.S.; Jordan, K.D.; Kay, B.D.; JA, J.A. LaVerne.; Lymar, S.V.; Madey, T.E.; McCurdy, C.W.; Meisel, D.; Mukamel, S.; Nilsson, A.R.; Orlando, T.M.; Petrik, N.G.; Pimblott, S.M.; Rustad, J.R.; Schenter, G.K.; Singer, S.J.; Tokmakoff, A.; Wang, L.S.; Wittig, C.; Zwier, T.S. *Chem. Rev.* **2005**, *105*, 355.
(4) Elles, C.G.; Jailaubekov, A.E.; Crowell, R.A.; Bradforth, S.E. *J. Chem. Phys.* **2006**, *125*, 44515.
(5) Elles, C.G.; Shkrob, I.A.; Crowell, R.A.; Bradforth, S.E. *J. Chem. Phys.* **2007**, *126*, 64503.
(6) Schnitker, Jürgen.; Rossky, P.J. *J. Chem. Phys.* **1987**, *86*, 3471.
(7) Boero, M.; Parrinello, M.; Terakura, K.; Ikeshoji, T.; Liew, C.C. *Phys. Rev. Lett.* **2003**, *90*, 226403.
(8) Tachikawa, Hiroto. *J. Phys. Chem. A* **2004**, *108*, 7853.
(9) Tachikawa, H. *J. Phys. Chem. A* **2002**, *106*, 6915.
(10) Furuhama, A.; Dupuis, M.; Hirao, K. *J. Chem. Phys.* **2006**, *124*, 164310.
(11) Novakovskaya, Y.V. *Int. J. Quantum Chem.* **2007**, *107*, 2763.
(12) VandeVondele, J.; Pieniazek, P.A.; Krylov, A.I.; Bradforth, S.E.; Jungwirth, P., to be published.
(13) Nielsen, S. O.; Michael, B.D.; Hart, E.J. *J. Phys. Chem.* **1976**, *2482*, 80.
(14) VandeVondele, J.; Sprik, M. *Phys. Chem. Chem. Phys.* **2005**, *7*, 1363.
(15) Pieniazek, P.A.; Krylov, A.I.; Bradforth, S.E. *J. Chem. Phys.* **2007**, *127*, 044317.
(16) Ng, C.Y.; Trevor, D.J.; Tiedemann, P.W.; Ceyer, S.T.; Kronebusch, P.L.; Mahan, B.H.; Lee, Y.T. *J. Chem. Phys.* **1977**, *67*, 4235.
(17) de Visser, S. P.; de Koning, L.J.; Nibbering, N.M.M. *J. Phys. Chem.* **1995**, *99*, 15444.
(18) Tomoda, S.; Achiba, Y.; Kimura, K. *Chem. Phys. Lett.* **1982**, *87*, 197.

(19) Moncrieff, D.; Hillier, I.H.; Saunders, V.R. *Chem. Phys. Lett.* **1982**, *89*, 447.
(20) Sato, K.; Tomoda, S.; Kimura, K. *Chem. Phys. Lett.* **1983**, *95*, 579.
(21) Curtiss, L.A. *Chem. Phys. Lett.* **1983**, *96*, 442.
(22) Tomoda, S.; Kimura, K. *Chem. Phys.* **1983**, *82*, 215.
(23) Curtiss, L.A. *Chem. Phys. Lett.* **1984**, *112*, 409.
(24) Gill, P.M.W.; Radom, L. *J. Am. Chem. Soc.* **1988**, *110*, 4931.
(25) Sodupe, M.; Oliva, A.; Bertran, J. *J. Am. Chem. Soc.* **1994**, *116*, 8249.
(26) Barnett, R.N.; Landman, U. *J. Phys. Chem.* **1995**, *99*, 17305.
(27) Barnett, R.N.; Landman, U. *J. Phys. Chem. A* **1997**, *107*, 2763.
(28) Sodupe, M.; Bertran, J.; Rodrguez-Santiago, L.; Baerends, E.J. *J. Phys. Chem. A* **1999**, *103*, 166.
(29) Müller, I.B.; Cederbaum, L.S. *J. Chem. Phys.* **2006**, *125*, 204305.
(30) Löwdin, P.O. *Rev. Mod. Phys.* **1963**, *35*, 496.
(31) Davidson, E.R.; Borden, W.T. *J. Phys. Chem.* **1983**, *87*, 4783.
(32) Russ, N.J.; Crawford, T.D.; Tschumper, G.S. *J. Chem. Phys.* **2005**, *120*, 7298.
(33) Sinha, D.; Mukhopadhyay, D.; Mukherjee, D. *Chem. Phys. Lett.* **1986**, *129*, 369.
(34) Sinha, D.; Mukhopadhya, D.; Chaudhuri, R.; Mukherjee, D. *Chem. Phys. Lett.* **1989**, *154*, 544.
(35) Chaudhuri, R.; Mukhopadhyay, D.; Mukherjee, D. *Chem. Phys. Lett.* **1989**, *162*, 393.
(36) Stanton, J.F.; Gauss, J. *J. Chem. Phys.* **1999**, *111*, 8785.
(37) Sekino, H.; Bartlett, R.J. *Int. J. Quantum Chem. Symp.* **1984**, *18*, 255.
(38) Koch, H.; Jensen, H.J.Aa.; Jørgensen, P.; Helgaker, T. *J. Chem. Phys.* **1990**, *93*, 3345.
(39) Stanton, J.F.; Bartlett, R.J. *J. Chem. Phys.* **1993**, *98*, 7029.
(40) Glendening, E. D.; Badenhoop, J. K.; Reed, A. E.; Carpenter, J. E.; Bohmann, J. A.; Morales, C. M.; Weinhold, F. *NBO 5.0*; *Theoretical Chemistry Institute*; University of Wisconsin: Madison, WI, 2001.
(41) Shao, Y.; Molnar, L. F.; Jung, Y.; Kussmann, J.; Ochsenfeld, C.; Brown, S.; Gilbert, A. T. B.; Slipchenko, L. V.; Levchenko, S. V.; O'Neil, D. P.; Distasio, R. A., Jr.; Lochan, R. C.; Wang, T.; Beran, G. J. O.; Besley, N. A.; Herbert, J. M.; Lin, C. Y.; Van Voorhis, T.; Chien, S. H.; Sodt, A.; Steele, R. P.; Rassolov, V. A.; Maslen, P.; Korambath, P. P.; Adamson, R. D.; Austin, B.; Baker, J.; Bird, E. F. C.; Daschel, H.; Doerksen, R. J.; Drew, A.; Dunietz, B. D.; Dutoi, A. D.; Furlani, T. R.; Gwaltney, S. R.; Heyden, A.; Hirata, S.; Hsu, C.-P.; Kedziora, G. S.; Khalliulin, R. Z.; Klunziger, P.; Lee, A. M.; Liang, W. Z.; Lotan, I.; Nair, N.; Peters, B.; Proynov, E. I.; Pieniazek, P. A.; Rhee, Y. M.; Ritchie, J.; Rosta, E.; Sherrill, C. D.; Simmonett, A. C.; Subotnik, J. E.; Woodcock, H. L., III; Zhang, W.; Bell, A. T.; Chakraborty, A. K.; Chipman, D. M.; Keil, F. J.; Warshel, A.; Herhe, W. J.; Schaefer, H. F., III; Kong, J.; Krylov, A. I.; Gill, P. M. W.; Head-Gordon, M. *Phys. Chem. Chem. Phys.* **2006**, *8*, 3172.
(42) (a) Feller, D. J. *Comp. Chem.* **1996**, *17*, 1571. (b) Schuchardt, K. L.; Didier, B. T.; Elsethagen, T.; Sun, L.; Gurumoorthi, V.; Chase, J.; Li, J.; Windus, T. L. *Chem. Inf. Model.* **2007**, *47*, 1045.
(43) VandeVondele, J.; Krack, M.; Mohamed, F.; Parrinello, M.; Chassaing, T.; J. Hutter, J. *Comp. Phys. Commun.* **2005**, *167*, 103.
(44) Goedecker, S.; Teter, M.; Hutter, J. Phys. Rev. B 1996.
(45) Zhang, Y.; Yang, W, *J. Chem. Phys.* **1998**, *109*, 2604.
(46) Polo, V.; Kraka, E.; Cremer, D. *Mol. Phys.* **2002**, *100*, 1771.
(47) Lundber, M.; Siegbahn, P. E. M. *J. Chem. Phys.* **2005**, *122*, 1.
(48) d'Avezac, M.; Calandra, M.; Mauri, F. *Phys. Rev. B* **2005**, *71*, 205210.
(49) VandeVondele, J.; Sprik, M. *Phys. Chem. Chem. Phys.* **2005**, *7*, 1363.
(50) Mantz, Y.A.; Gervasio, F.L.; Laino, T.; Parrinello, M. *J. Phys. Chem. A* **2007**, *111*, 105.
(51) Cheng, B.-M.; Chew, E. P.; Liu, C.-P.; Bahou, M.; Lee, Y.-P.; Yung, Y. L.; Gerstell, M. F. *Geophys. Res. Lett.* **1999**, *26*, 3657.
(52) Bally, T.; Sastry, G.N. *J. Phys. Chem. A* **1997**, *101*, 7923.
(53) Vanovschi, V.; Krylov, A. I.; Wenthold, P. G. *Theor. Chim. Acta* **2008**, *120*, 45.
(54) Vydrov, O. A.; Scuseria, G. E. *J. Chem. Phys.* **2006**, *124*, 191101.
(55) Pople, J. A.; Gill, P. M. W.; Handy, N. C. *Int. J. Quantum Chem.* **1995**, *56*, 303.
(56) Tawada, Y.; Tsuneda, T.; Yanagisawa, S.; T. Yanai, T.; Hirao, K.K. *J. Chem. Phys.* **2004**, *120*, 8425.
(57) Livshits, E.; R. Baer, R. *Phys. Chem. Chem. Phys.* **2007**, *9*, 2932.
(58) Cohenand, A. J.; Mori-S'anchez, P.; Yang, W. *J. Chem. Phys.* **2007**, *126*, 191109.
(59) Becke, A. D.; Johnson, E. R. *J. Chem. Phys.* **2007**, *127*, 124108.
(60) Chai, J.-D.; Head-Gordon, M. *J. Chem. Phys.* **2008**, *128*, 084106.
(61) Pieniazek, P. A.; Arnstein, S. A.; Bradforth, S. E.; Krylov, A. I.; Sherrill, C. D. *J. Chem. Phys.* **2007**, *127*, 164110.
(62) Pieniazek, P. A.; Sundstrom, E. J.; Bradforth, S. E.; Krylov, A. I. , to be published, 2008.
(63) Pieniazek, P. A.; Bradforth, S. E.; Krylov, A. I. *J. Phys. Chem. A* **2006**, *110*, 4854.
(64) Birks, J. B. *Photophysics of Aromatic Molecules*; Wiley: New York, 1970.
(65) East, A. L. L.; Lim, E. C. *J. Chem. Phys.* **2000**, *113*, 8981.
(66) Banna, M. S.; McQuaide, B. H.; Malutzki, R.; Schmidt, V. *J. Chem. Phys.* **1986**, 84.
(67) Reutt, J. E.; Wang, L. S.; Lee, Y. T.; Shirley, D. A. *J. Chem. Phys.* **1986**, *85*, 6928.
(68) Hotop, H.; Patterson, T. A.; Lineberger, W. C. *J. Chem. Phys.* **1974**, *60*, 1806.
(69) Smith, J. R.; Kim, J. B.; Lineberger, W. C. *Phys. Rev. A* **1997**, *55*, 2036.
(70) Das, B.; Farley, J. W. *J. Chem. Phys.* **1991**, *95*, 8809.
(71) Huber, K. P.; Herzberg, G. Constants of Diatomic Molecules (data prepared by Gallagher, J. W. and Johnson R. D., III); *NIST Chemistry WebBook, NIST Standard Reference Database Number 69*; Linstrom, P. J., Mallard, W. G. Eds; National Institute of Standards and Technology: Gaithersburg, MD (http://webbook.nist.gov), July 2001.

JP802140C